



ARTICLE

## Overall Assessment of Heat Transfer for a Rarefied Flow in a Microchannel with Obstacles Using Lattice Boltzmann Method

Siham Hammid<sup>1</sup>, Khatir Naima<sup>2</sup>, Omolayo M. Ikumapayi<sup>3</sup>, Cheikh Kezrane<sup>4</sup>, Abdelkrim Liazid<sup>4</sup>, Jihad Asad<sup>5</sup>, Mokdad Hayawi Rahman<sup>6</sup>, Farhan Lafta Rashid<sup>7</sup>, Naseer Ali Hussien<sup>8</sup> and Younes Menni<sup>2,9,\*</sup>

<sup>1</sup>Laboratory of Development in Mechanics and Materials (LDMM), Zian Achour University, Djelfa, PB 3117, Algeria

<sup>2</sup>Department of Technology, University Center Salhi Ahmed Naama (Ctr. Univ. Naama), P. O. Box 66, Naama, 45000, Algeria

<sup>3</sup>Department of Mechanical and Mechatronics Engineering Afe Babalola University, Ado Ekiti, 360101, Nigeria

<sup>4</sup>Departement of Physics, Faculty of Science, Abou Bekr Belkaid University, Tlemcen, 13000, Algeria

<sup>5</sup>Department of Physics, Faculty of Applied Sciences, Palestine Technical University-Kadoorie, Tulkarm, Palestine

<sup>6</sup>Aeronautical Technical Engineering, Al-Farahidi University, Baghdad, 10011, Iraq

<sup>7</sup>Mechanical Engineering Department, University of Kerbala, Karbala, 56001, Iraq

<sup>8</sup>Information and Communication Technology Research Group, Scientific Research Center, Al-Ayen University, Thi-Qar, Iraq

<sup>9</sup>National University of Science and Technology, Dhi Qar, Iraq

\*Corresponding Author: Younes Menni. Email: [menni.younes@cuniv-naama.dz](mailto:menni.younes@cuniv-naama.dz)

Received: 18 January 2023 Accepted: 04 May 2023 Published: 22 September 2023

### ABSTRACT

The objective of this investigation is to assess the effect of obstacles on numerical heat transfer and fluid flow momentum in a rectangular microchannel (MC). Two distinct configurations were studied: one without obstacles and the other with alternating obstacles placed on the upper and lower walls. The research utilized the thermal lattice Boltzmann method (LBM), which solves the energy and momentum equations of fluids with the BGK approximation, implemented in a Python coding environment. Temperature jump and slip velocity conditions were utilized in the simulation for the MC and extended to all obstacle boundaries. The study aims to analyze the rarefaction effect, with Knudsen numbers (Kn) of 0.012, 0.02, and 0.05. The outcomes indicate that rarefaction has a significant impact on the velocity and temperature distribution. The presence of nine obstacles led to slower fluid movement inside the microchannel MC, resulting in faster cooling at the outlet. In MCs with obstacles, the rarefaction effect plays a crucial role in decreasing the Nusselt number (Nu) and skin friction coefficient (Cf). Furthermore, the study demonstrated that the obstacles played a crucial role in boosting fluid flow and heat transfer in the MC. The findings suggest that the examined configurations could have potential applications as cooling technologies in micro-electro-mechanical systems and microdevice applications.

### KEYWORDS

Microfluid; rarefied flow; LBM; microchannel; Knudsen number; numerical simulation



## Nomenclature

$f$	Density momentum distribution function
$g$	Internal energy distribution function
$c_s$	Lattice speed of sound ( $ms^{-1}$ )
$T_{in}$	Inlet temperature ( $K$ )
$T_w$	Wall temperature ( $K$ )
$u_{in}$	Inlet velocity ( $ms^{-1}$ )
$H$	Non-dimensional height of microchannel
$L$	Non-dimensional length of microchannel
$P$	Pressure
$C_{jump}$	Temperature jump coefficient
$T_{bulk}$	Bulk temperature
$k$	Thermal conductivity ( $W/m\cdot K$ )
$k_n$	Knudsen number
$Re$	Reynolds number
$Pr$	Prandtl number
$Nu$	Nusselt number
$B$	Non-dimensional parameter
$e$	Internal energy
$\rho$	Density ( $kg/m^3$ )
$t_f$	Relaxation time for velocity
$t_g$	Relaxation time for temperature
$\nu$	Kinematic viscosity
$\alpha$	Thermal diffusivity ( $m^2s^{-1}$ )
$\mu$	Viscosity ( $kg\cdot m^{-1}s^{-1}$ )
$w$	Weight factor
$LBM$	Lattice Boltzmann method
$TLBM$	Thermal lattice Boltzmann method
$BGK$	Bhatnagar, Gross, and Krook
$i$	Lattice direction
$eq$	Equilibrium
$x$	Position
$t$	Time
$in$	Inlet
$n$	Outlet
$w$	Wall

## 1 Introduction

Microfluidic devices have been developing rapidly in recent years, and have been increasing in several applications such as drug delivery and cell sorting. Microfluidic devices have advantages over traditional devices, such as low energy cost and separation efficiency [1]. In addition to parallel processing, low material usage, and energy efficiency [2]. Moreover, The control of flows [2] in microchannels (MCs) and heat transfer is considered a complex process [3] and is one of the most important research fields in microfluidics [4]. Microchannels have various implementations in several fields as the cooling technology for addressing heat dissipation issues obtained via high heat flux devices [5]. For example, MC heat sinks are considered cutting-edge cooling technology for electronic

systems according to their height of heat generation [6]. The heat transfer mechanism differs from the micro size to the macro size.

The Knudsen number (Kn), which is defined as the ratio of the particle mean free path to the characteristic length of the flow, serves as an indicator of the rarefaction effect [7]. The Kn number provides a way to categorize fluid flows in the micro-scale into four distinct regimes, each with unique characteristics. These regimes are classified as: continuum flow (for Kn numbers below 0.001), slip flow (for Kn numbers between 0.001 and 0.1), transition flow (for Kn numbers between 0.1 and 10), and free-molecular flow (for Kn numbers greater than 10). This categorization is based on the relative importance of viscous and molecular forces in determining the behavior of the fluid. The Kn number serves as a useful tool for predicting the regime of fluid flow and designing systems that operate in specific flow regimes [8,9].

In microflows, the slip boundary plays a critical role and cannot be neglected when analyzing the fluid's flow and thermal behaviors [10,11]. The lattice Boltzmann method (LBM) can be used in microfluidics as an important computational tool [12,13]. According to the high level of parallel ability and the simple algorithm formulation [14], particularly the explicit formulation. The LBM method shows excellent implementation [15] as well as can handle complex boundary conditions [6]. Furthermore, the thermal LBM has been acknowledged as a powerful technique for investigating MC flows that incorporate slip boundary conditions [16]. The LBM method includes two steps collision and streaming [13]. Various models of LBM have been developed to increase the performance of the thermal field simulation. One approach that has been proposed for modeling microscale flows is the double population method, which involves the use of two distinct distribution functions. Specifically, this approach utilizes a density-momentum distribution function for the fluid domain and an internal energy distribution function for the thermal field [11,17].

Numerous studies have investigated the behavior of heat transfer and fluid flow in MCs utilizing the thermal LBM while taking into account slip velocity and temperature jump. For instance, Niu et al. [18] used the thermal LBM to simulate microthermal flow with velocity slip and temperature jump. Similarly, Liu et al. [19] investigated gas flow in a long MC with the LBM and examined the effects of slip and transition flow. Their results showed that the rarefaction effect becomes increasingly significant as the Kn number increases. Hatam et al. [20] studied Cu-H<sub>2</sub>O heat transfer in a MC heat sink and demonstrated that increasing the interactions 'nanoparticles-solid phase' leads to an increase in channel aspect ratio, resulting in an elevated Nusselt number. Finally, Ghadirzadeh et al. [21] utilized the LBM to simulate laminar nanofluid flows within an annular MC in a slip flow regime. These studies provide valuable insights into the behavior of fluids in MCs under various conditions and have advanced our understanding of the mechanisms governing heat transfer and fluid flow in these systems.

Knupp et al. [22] analyzed slip flow in laminar gaseous flow with heat transfer in circular MCs. The study found a decrease in Nu numbers as the Kn number increased. Ahangar et al. [23] used LBM to investigate slip and transient flow regimes in MCs. The study found that in the slip regime, the velocity increased with the Kn number at the center and at the exit of the MC in the transient regime. Alipour Lalami et al. [24] employed LBM with slip boundary and temperature jump to examine heat transfer of nanofluids at conjugate heat in a wide MC with a thick wall. The study found that higher Re values caused an increase in the average Nu number on superhydrophobic surfaces. Finally, Rehman et al. [25] investigated fluid flow in a rectangular channel with a partially heated region by a circular, heated cylinder placed between channels as an obstacle. The study considered four different cases where

rectangular ribs were installed and found that the circular obstacle showed the highest drag force when rectangular ribs were present on both the lower and upper walls heated.

Ashraf et al. [26] investigated the behavior of an oscillating mixed convection flow over a horizontal circular cylinder. The study revealed that buoyancy forces play a significant role in accelerating the fluid flow and increasing the velocity of fluid particles. Qiu et al. [27] examined the heat dissipation model of a copper MC heat sink, considering the impact of the Nu number on heat transfer. Their results indicated that the Nu number is a crucial factor affecting the heat transfer performance. Ma et al. [28] simulated 3D laminar flow in a rectangular MC and found that low Re numbers can considerably influence the local Nu numbers in the thermal zone. Overall, these studies provide insights into the complex nature of heat transfer and fluid flow in MCs, highlighting the importance of considering various factors such as buoyancy forces, Nu number, and Re number for achieving optimal heat transfer performance.

In recent years, improving the heat transfer in microdevices has become a significant area of research, especially with the rapid advancement of Micro Electro Mechanical Systems (MEMS) [12,13]. The demand for more efficient designs and technologies to enhance heat transfer efficiency in heat transfer systems has also increased. Slip velocity conditions and temperature jump implementation are some of the methods that have been explored. The Lattice Boltzmann Method (LBM) has been recognized as a useful method to simulate microflow due to its mesoscale characteristics [14]. LBM has several attractive features, including superior representation of microscopic interactions. The most recent and useful LBM framework for dealing with thermal flows is the thermal lattice Boltzmann method with a double distribution function [17]. In the literature, various studies have been conducted on microscale heat transfer, such as Ashraf et al. [29], who examined the impact of variable surface temperature on periodic mixed convection using a thermally and electrically conducting cone in a porous medium. The study by Lori et al. [30] investigated the heat transfer and fluid flow in solid ribs and alternating vertical porous with microchannel heat sinks, showing that the average Nusselt number of the porous-rib microchannel was more significant than the solid case. Another study by Lobasov et al. [4] explored the influence of temperature jump and velocity slip on heat transfer in the microchannel and found that the heat flux density and average heat transfer coefficient increased as the slip length increased.

In the study by Ashraf et al. [29], the impact of variable surface temperature on periodic mixed convection was analyzed through the use of a thermally and electrically conducting cone positioned in a porous medium. The results indicated that there was an increase in temperature distribution as the Pr number values rose. Meanwhile, Lori et al. [30] explored heat transfer and fluid flow in solid ribs and porous material that alternated vertically with MC heat sinks. According to their findings, the average Nu number was greater in the porous-rib MC than in the solid case. Lastly, Lobasov et al. [4] focused on investigating the effects of temperature jump and velocity slip on heat transfer in a MC. Their research revealed that the heat flux density and average heat transfer coefficient increased with an increase in slip length. These three studies provide important insights into the diverse factors that can impact heat transfer in different systems.

Microdevices have witnessed significant advancements in recent times, with Micro Electro Mechanical Systems (MEMS) driving a lot of innovation [12,13]. However, there is a pressing need for more efficient and better-designed heat transfer systems to improve heat transfer in microdevices [31]. Two crucial factors that can impact the performance of such systems are the slip velocity condition and temperature jump implementation. A promising approach that has gained considerable attention in this context is the LBM, which offers superior representation of microscopic interactions [32]. Of

all the LBM frameworks available, the thermal LBM with a double distribution function [17] is the most recent and useful for simulating microflows owing to its mesoscale characteristics [14]. LBM has demonstrated its superiority in modeling rarefied gas flow in microchannels [8]. These observations highlight the potential of LBM in enhancing heat transfer in microdevices and the need for further research in this area.

The present study aims to provide a numerical investigation of laminar fluid flow and forced convective heat transfer in a rectangular MC, both with and without obstacles placed on the walls. To conduct this study, we employed the thermal LBM with the BGK model, while implementing slip velocity and temperature jump on both the walls and the obstacles. The novelty of this study lies in its focus on the impact of obstacles present in the MC walls and how they can enhance fluid flow and heat transfer. Additionally, the study examines the application of thermal LBM with slip velocity and temperature jump on MC and obstacle walls. To this end, the MC was simulated with different obstacle positions, and the effects of the Kn number, the implementation of obstacles on fluid flow and heat transfer, and the Nu number in the MC were analyzed. The results of this study hold significant implications for the design of more efficient microfluidic devices with enhanced heat transfer.

## 2 Mathematical Modelling and Numerical Methods

### 2.1 Problem Statement

In the present numerical investigations, the laminar fluid flow through the 2D rectangular MCs without and with alternating obstacles is studied with the LBM to analyze the convection heat transfer and fluid flow. A unit length  $L$  of the MC is considered. In the first case, the MC is without obstacles. The second case is with three obstacles, two from them at the top and one obstacle at the bottom. In the third case, six obstacles are placed at the top wall and three obstacles at the bottom wall, as shown in Fig. 1. The inlet velocity and flow temperature remain constant at the inlet of the microchannel. The MC walls are at rest. In addition, the wall's temperature was kept constant and the same and equal  $T_w = 10T_{in}$ . The dimensions  $L_0$  and  $L_1$  correspond to the length of the obstacle in the second and third cases, respectively. In addition,  $H$  is the width of MC and  $W_0$  is the obstacle's width. The dimension  $d_0$  expresses the distance between the two obstacles located in the upper wall in the second case and also the obstacle distance from the inlet on the lower wall and  $d_1$  represents the distance separating obstacles in the third case. Fig. 1 shows the MC's configurations.

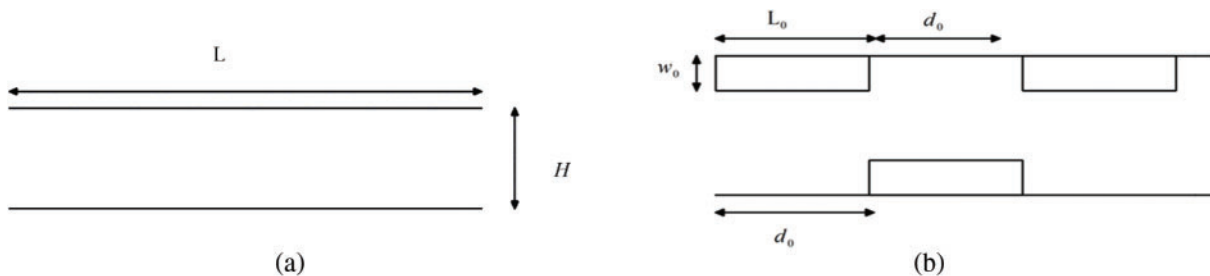
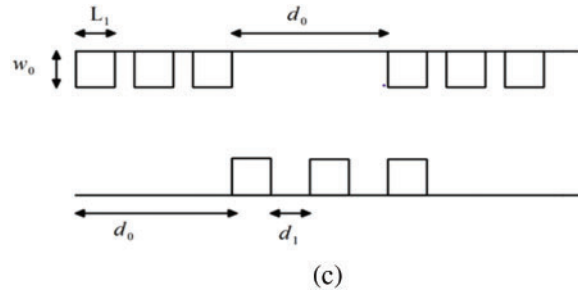


Figure 1: (Continued)



**Figure 1:** MC configurations with (a) no, (b) three, (c) nine obstacles

## 2.2 Thermal Lattice Boltzmann

The microscale level presents unique challenges for computational fluid dynamics (CFD) techniques. The lattice Boltzmann method (LBM) has emerged as a promising alternative due to its simplicity and ability to handle complex microstructures [10]. In particular, the thermal lattice Boltzmann method (TLBM) has gained traction in heat transfer and fluid flow problems owing to its recent establishment and several potential applications [33]. The double distribution function approach, which uses two distribution functions to represent the velocity and temperature fields, respectively, is particularly useful in this context [15,34]. This study employs the TLBM with a double distribution function and BGK model to investigate fluid flow and temperature. The mathematical formalism is represented by the discrete Eqs. (1) and (2) [12]. The use of TLBM in this study highlights its potential for enhancing heat transfer and fluid flow in microscale systems, and its mathematical formalism opens up avenues for further research in this area.

$$f_i(X + c_i \Delta t, t + \Delta t) - f_i(X, t) = -\frac{1}{\tau_f} [f_i(X, t) - f_i^{eq}(X, t)] \quad (1)$$

$$g_i(X + c_i \Delta t, t + \Delta t) - g_i(X, t) = -\frac{1}{\tau_g} [g_i(X, t) - g_i^{eq}(X, t)] \quad (2)$$

In this study, we utilize a lattice model represented by a two-dimensional  $D2Q9$  lattice connected by eight links, as depicted in Fig. 2. This lattice model serves as the foundation for our analysis and enables us to investigate the phenomena of interest accurately. By employing this specific lattice model, we can examine the behavior of the system in a controlled and precise manner, which is essential for drawing meaningful conclusions from our research.

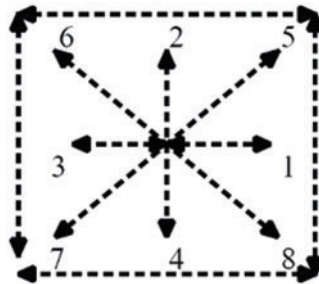


**Figure 2:**  $D2Q9$  square lattice model

The equilibrium distribution functions of  $f_i$  and  $g_i$  are denoted by  $f_i^{eq}$  and  $g_i^{eq}$ , respectively. For a  $D2Q9$  square lattice, these functions can be derived as follows [12,35]:

$$f_i^{eq} = \omega_i \rho \left[ 1 + \frac{3(c_i u)}{c^2} + \frac{9(c_i u)^2}{2c^4} - \frac{3(u u)}{2c^2} \right]$$

$$g_0^{eq} = -\omega_0 \rho \varepsilon \frac{3(u u)}{2c^2} \quad (3)$$

$$g_{1,2,3,4}^{eq} = \omega_{1,2,3,4} \rho \varepsilon \left[ 1.5 + \frac{3(c_i \cdot u)}{2c^2} + \frac{9(c_i \cdot u)^2}{2c^4} - \frac{3(u u)}{2c^2} \right]$$

$$g_{5,6,7,8}^{eq} = \omega_{5,6,7,8} \rho \varepsilon \left[ 3 + \frac{6(c_i \cdot u)}{c^2} + \frac{9(c_i \cdot u)^2}{2c^4} - \frac{3(u u)}{2c^2} \right] \quad (4)$$

We can express the discrete velocity vector for the  $D2Q9$  lattice, which consists of a stationary central node connected to eight neighboring nodes in space, as follows:

$$c_i = (0, 0) \quad (i = 0)$$

$$c_i = \left[ \cos \frac{(i-1)\pi}{2}, \sin \frac{(i-1)\pi}{2} \right] c \quad i = 1, 2, 3, 4$$

$$c_i = \left[ \cos \frac{(i-1)\pi}{4}, \sin \frac{(i-1)\pi}{4} \right] c\sqrt{2} \quad i = 5, 6, 7, 8 \quad (5)$$

In the  $D2Q9$  discrete velocity model, the weighting coefficient is given by:

$$w_0 = \frac{4}{9} \text{ for } i = 0, w_i = \frac{1}{9} \text{ for } i = 1, 2, 3, 4, w_i = \frac{1}{36} \text{ for } i = 5, 6, 7, 8$$

By utilizing the distribution function, we can calculate various macroscopic quantities, such as density, velocity, and temperature. These quantities are crucial in describing the behavior of the system under study and provide valuable insights into the underlying physical processes. The ability to calculate these macroscopic quantities accurately and efficiently from the distribution function is a significant advantage of this approach and allows us to gain a better understanding of the system's dynamics.

$$\rho = \sum_i f_i \quad (6)$$

$$\rho \vec{u} = \sum_i f_i \vec{c}_i \quad (7)$$

$$\rho \varepsilon = \rho RT = \sum_i g_i \quad (8)$$

The pressure can be directly obtained from the density and sound speed of the lattice  $c_s^2$  as [12]:

$$P = \rho c_s^2 \quad (9)$$

One can establish a relationship between the relaxation time and the kinematic viscosity ( $\nu$ ) and thermal diffusivity ( $\alpha$ ). These two physical quantities play a crucial role in characterizing the dynamics of the system under study.

$$\nu = \frac{1}{3}(t_f - 0.5) \quad (10)$$

$$\alpha = \frac{1}{3}(t_s - 0.5) \quad (11)$$

## 2.3 Boundary Condition

### 2.3.1 Flow Boundary Conditions

The velocity is known at the inlet boundary but must be determined the density. The corrections performed by [36] were used to determine inlet density and unknown distribution functions:

$$\rho_{in} = \frac{1}{(1 - u_{in})} [f_0 + f_2 + f_4 + 2(f_3 + f_6 + f_7)] \quad (12)$$

$$f_1 = f_3 + \frac{2}{3}\rho_{in}u_{in} \quad (13)$$

$$f_5 = f_7 - \frac{1}{2}(f_2 - f_4) + \frac{1}{6}\rho_{in}u_{in} \quad (14)$$

$$f_8 = f_6 - \frac{1}{2}(f_4 - f_2) + \frac{1}{6}\rho_{in}u_{in} \quad (15)$$

The outlet velocity is unknown. Extrapolation is commonly utilized to obtain the unknown distribution functions at the east boundary [33], as shown by the Eqs. (16)–(18):

$$f_{3,n} = 2 \cdot f_{3,n-1} - f_{3,n-2} \quad (16)$$

$$f_{6,n} = 2 \cdot f_{6,n-1} - f_{6,n-2} \quad (17)$$

$$f_{7,n} = 2 \cdot f_{7,n-1} - f_{7,n-2} \quad (18)$$

Fluid velocity near the wall differs from wall speed. The slip boundary condition for the bottom wall is given by the Eqs. (19)–(23) [21]:

$$\rho_w = [f_0 + f_1 + f_3 + 2(f_7 + f_4 + f_8)] \quad (19)$$

$$f_2 = f_4 \quad (20)$$

$$f_5 = \frac{\rho_w(1 + u_x) - (f_0 + f_2 + f_4)}{2} - (f_1 + f_8) \quad (21)$$

$$f_6 = \frac{\rho_w(1 - u_x) - (f_0 + f_2 + f_4)}{2} - (f_3 + f_7) \quad (22)$$



$$u_x = \frac{kn(4u_{x,1} - u_{x,2})}{2 + 3kn} \quad (23)$$

After the fluid's velocity on the microchannel wall, the speeds of the first two network nodes are  $u_{x,1}$  and  $u_{x,2}$ . Similarly, the slip boundary for the top can be expressed as:

$$\rho_w = f_0 + f_1 + f_3 + 2(f_2 + f_5 + f_6) \quad (24)$$

$$f_4 = f_2 \quad (25)$$

$$f_7 = \frac{\rho_w(1 - u_x) - (f_0 + f_2 + f_4)}{2} - (f_3 + f_6) \quad (26)$$

$$f_8 = \frac{\rho_w(1 + u_x) - (f_0 + f_2 + f_4)}{2} - (f_1 + f_5) \quad (27)$$

$$u_x = \frac{kn(4u_{x,H-1} - u_{x,H-2})}{2 + 3kn} \quad (28)$$

### 2.3.2 Temperature Boundary Conditions

The inlet temperature is given by [10] as:

$$g_1 = \frac{1}{9}T_{in}(3 + 6u_x^2) - g_3 \quad (29)$$

$$g_5 = \frac{1}{36}T_{in}(6 + 6u_x^2) - g_7 \quad (30)$$

$$g_8 = \frac{1}{36}T_{in}(6 + 6u_x^2) - g_6 \quad (31)$$

An extrapolation can be used to obtain the outlet boundary condition for temperature [28]:

$$g_{3,n} = 2 \cdot g_{3,n-1} - g_{3,n-2} \quad (32)$$

$$g_{6,n} = 2 \cdot g_{6,n-1} - g_{6,n-2} \quad (33)$$

$$g_{7,n} = 2 \cdot g_{7,n-1} - g_{7,n-2} \quad (34)$$

Tian et al. [35] described a temperature jump boundary condition for the top wall as:

$$T_{y=H} = \frac{C_{jump}(4T_{H-1} - T_{H-2}) + 2T_w}{(2 + 3C_{jump})} \quad (35)$$

$$g_4 = 1.5T_{y=H}(\omega(2) + \omega(4)) - g_2 \quad (36)$$

$$g_7 = 3T_{y=H}(\omega(5) + \omega(7)) - g_5 \quad (37)$$

$$g_8 = 3T_{y=H}(\omega(6) + \omega(8)) - g_6 \quad (38)$$

Temperature jumps for the bottom wall are defined by the Eqs. (39)–(42):

$$T_{y=0} = \frac{C_{jump} (4T_1 - T_2) + 2T_W}{(2 + 3C_{jump})} \quad (39)$$

$$g_2 = 1.5T_{y=0}(\omega(2) + \omega(4)) - g_4 \quad (40)$$

$$g_5 = 3T_{y=0}(\omega(5) + \omega(7)) - g_7 \quad (41)$$

$$g_6 = 3T_{y=0}(\omega(6) + \omega(8)) - g_8 \quad (42)$$

The Number is expressed as [12]:

$$Nu(x) = \frac{k2H}{k(T_w - T_{bulk})} \left. \frac{\partial T}{\partial y} \right|_w \quad (43)$$

The local friction coefficient is determined by the equation:

$$C_f(x) = \frac{\mu (\partial u / \partial y)}{(1/2) \rho u_{bulk}^2} \Big|_w \quad (44)$$

## 2.4 Grid Independency

Table 1 represents the mesh independency study at  $x = 0.5L$  for  $Kn = 0.015$  for three different mesh sizes  $100 \times 25$ ,  $120 \times 30$ , and  $150 \times 37$ . The  $120 \times 30$  mesh was selected for the present study.

**Table 1:** Mesh independency

Mesh size	$100 \times 25$	$120 \times 30$	$150 \times 37$	$160 \times 40$	$170 \times 42$
$\frac{u}{u_{in}}$	0.0937	0.0887	0.0872	0.0835	0.0829
$\frac{T}{T_{in}}$	9.8614	9.8096	9.7888	9.714	9.700

## 2.5 Numerical Method and Validation

The present study was achieved under a python code environment to simulate heat transfer and fluid flow in a MC. The results were compared with those [12]. Velocity and temperature have without obstacles. From Fig. 3, the results show a good agreement.

The Nusselt number also shows a suitable agreement with various  $Kn$  numbers, as indicated in Fig. 4. The figures display the desired accuracy for employment developed code for the following simulation.

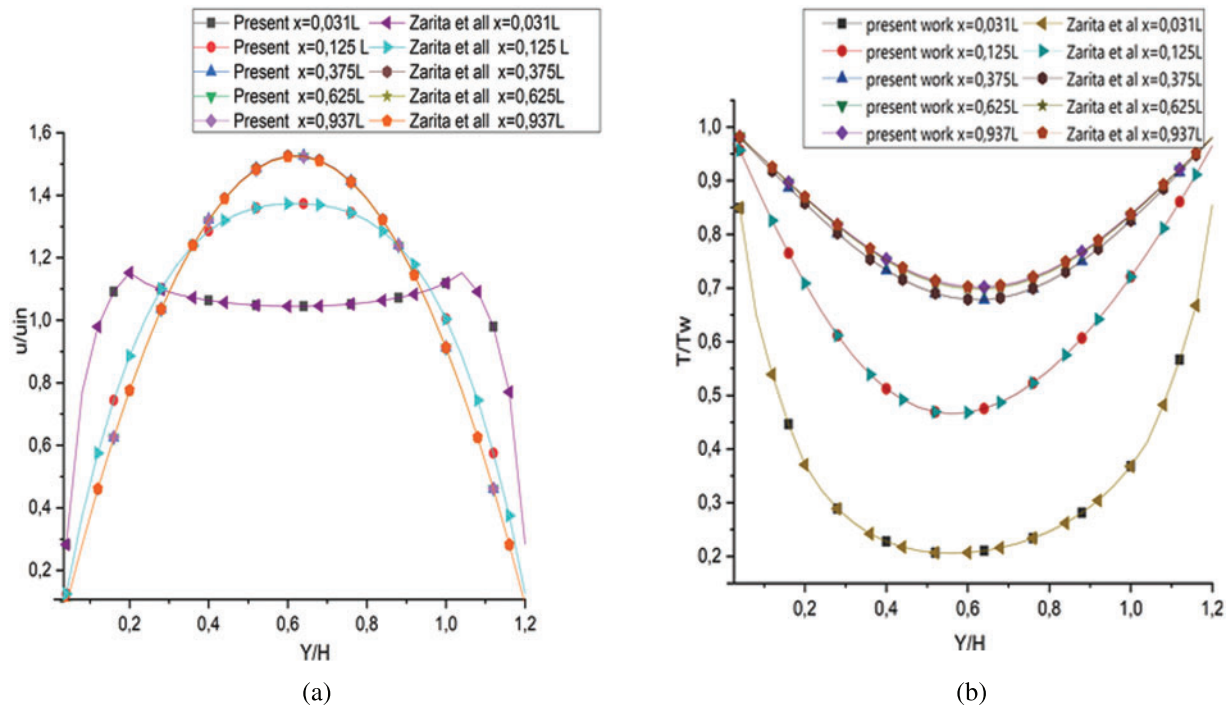


**Figure 3:** Comparison of temperature and velocity profiles for  $Kn = 0.015$  with [12]: (a) velocity, and (b) temperature

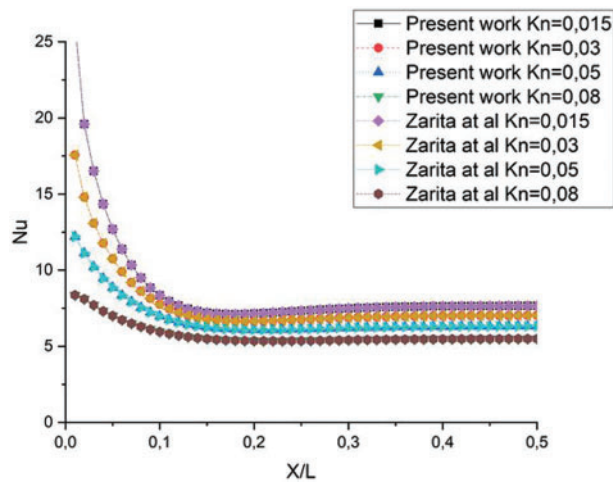
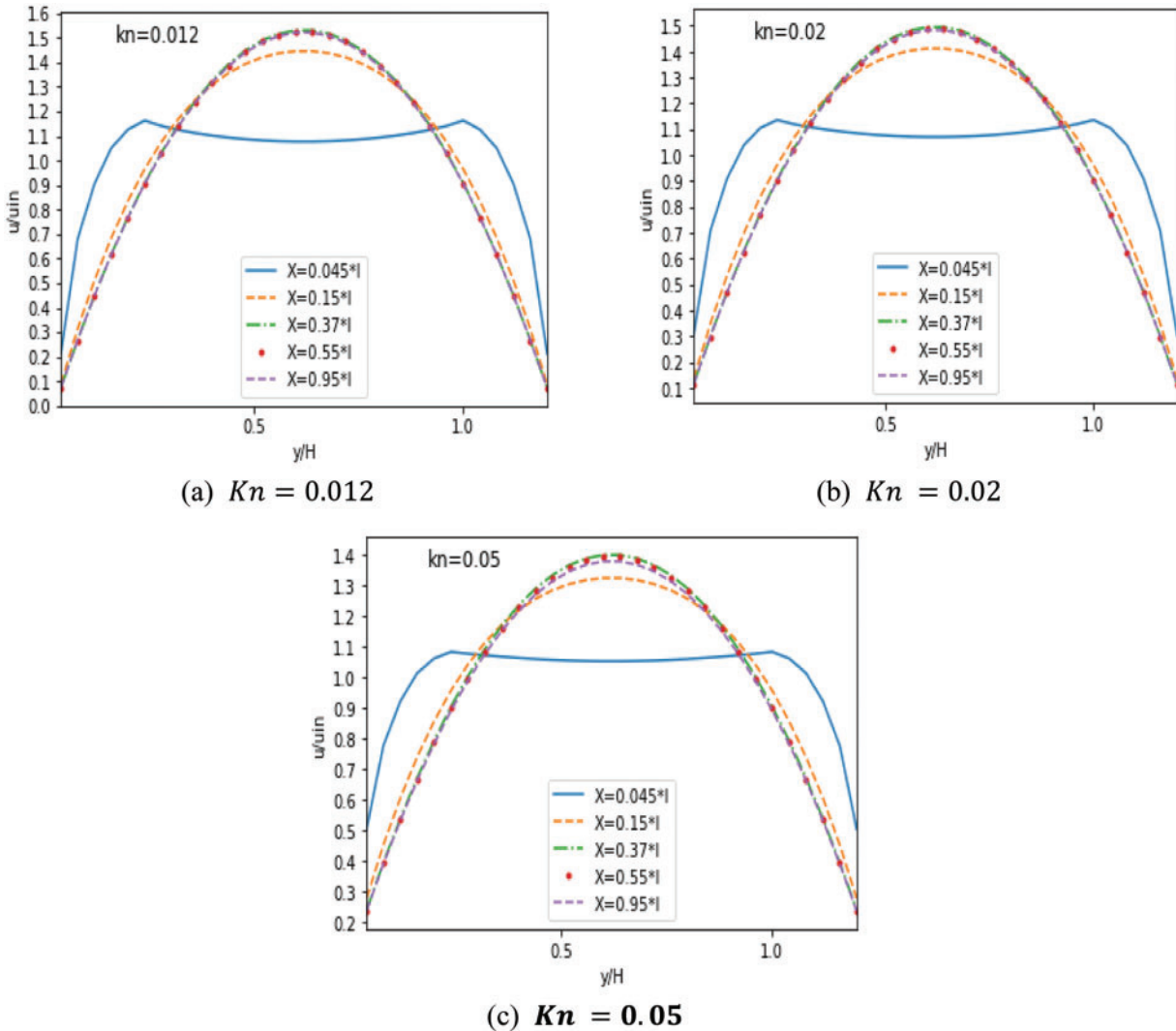


**Figure 4:** Comparison of Nusselt number for different  $Kn$  numbers with [12]

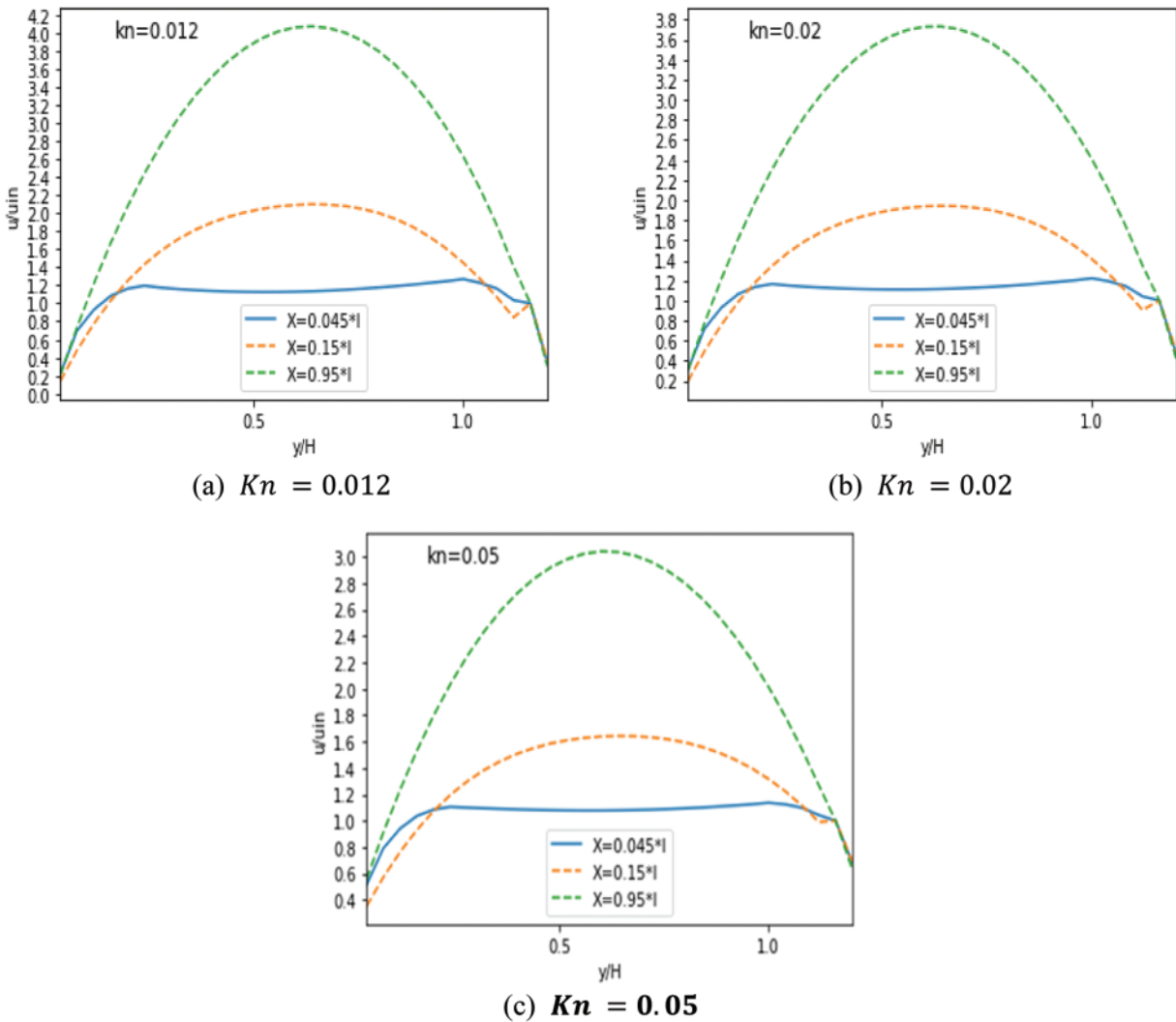
### 3 Results and Discussions

Figs. 5–7 represent the MC’s velocity distribution for  $Kn = 0.012 - 0.02$  and  $Kn = 0.05$ . In the absence of obstacles, the velocity decreases with the increase of  $Kn$  numbers. In case of obstacles, the velocity drops as the  $Kn$  number values grow, and the velocity values increase in the case of obstacle implementation. From the velocity profiles, the performance of obstacles plays a vital role in increasing

velocity. Also, the significant effect of obstacles on velocity distribution occurs in the case of three obstacles with low  $Kn$  numbers. However, the results indicated the importance of the rarefaction effect on velocity distribution, especially can notice their influence is more significant in the middle of MC than next to wall. Nonetheless, the findings demonstrate the significance of the rarefaction effect on the distribution of velocity. It is noteworthy that this influence is more prominent in the center as opposed to near the wall, as indicated by previous research [13]. Our analysis suggests that obstacles had a substantial impact on the increase in velocity.

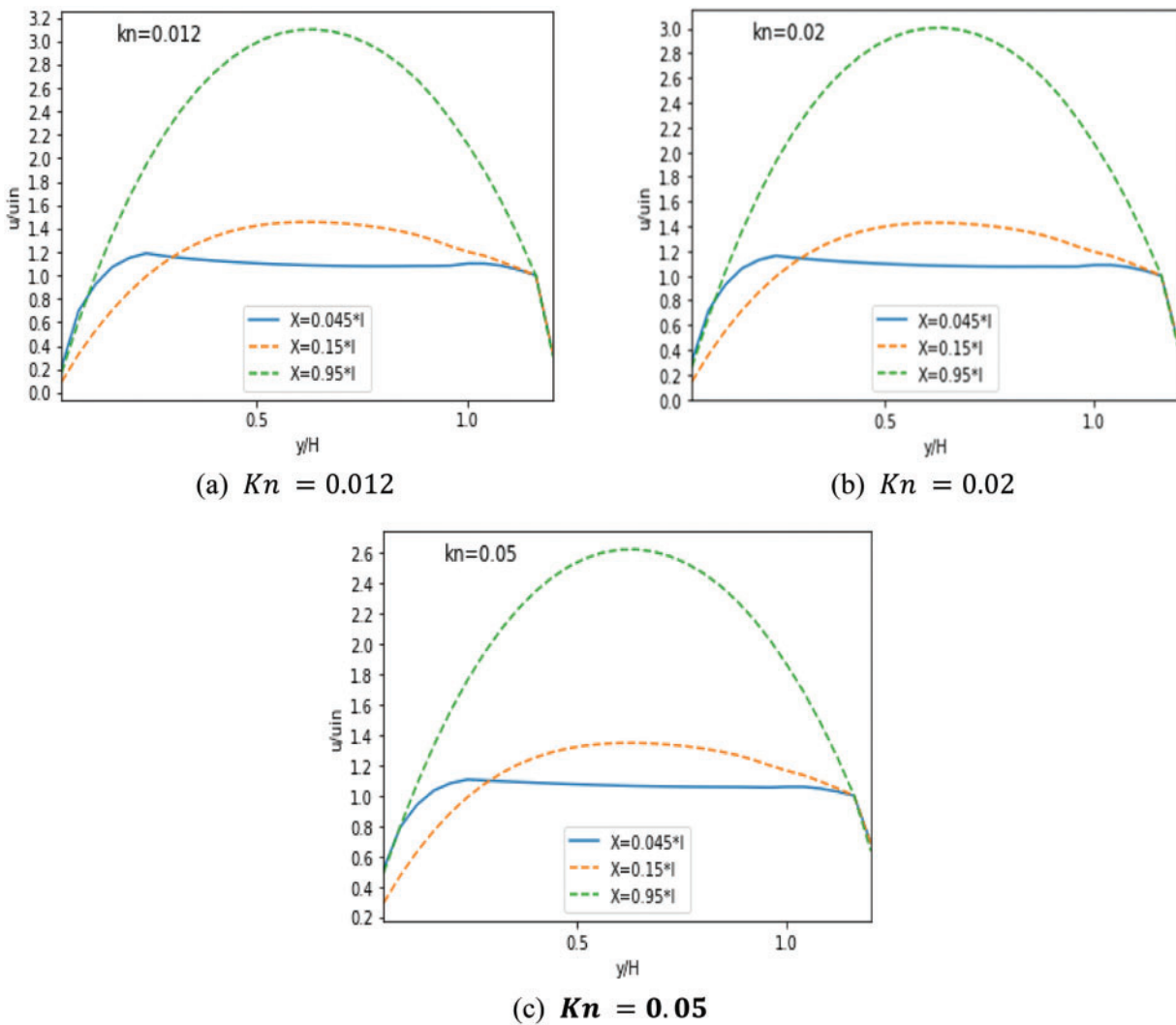


**Figure 5:** Velocity without obstacles for different  $Kn$  numbers



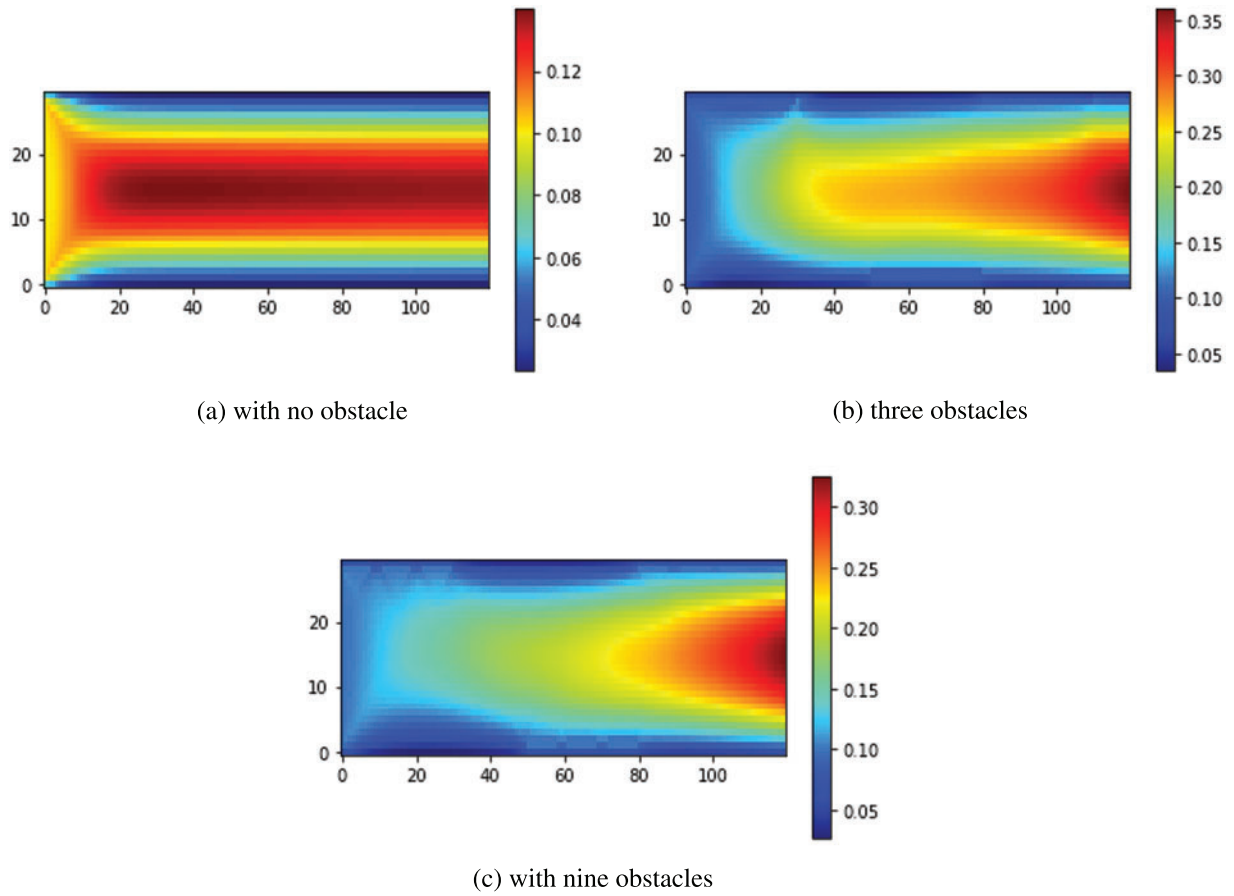
**Figure 6:** Velocity with three obstacles for different  $Kn$  numbers

Fig. 8 shows the velocity streamlines in various cases with  $Kn = 0.05$ . The velocity field increased rapidly in the developing region until it achieved a maximum in the center of the MC, as shown in the streamlined structures without obstacles in Fig. 4a. Also, the fluid near the wall maintains a minimum velocity. In the cases of obstacles, the velocity field rises slowly due to obstacles but with a high value compared to the first case. Furthermore, the developing region experienced a substantial deceleration in the third scenario. The velocity of the rarefied flow reached its peak value upon exiting the MC, which was higher than the velocity observed in the first scenario that had no obstacles. These findings demonstrate that the presence of obstacles had a significant impact on accelerating the velocity of the rarefied flow in the MC.



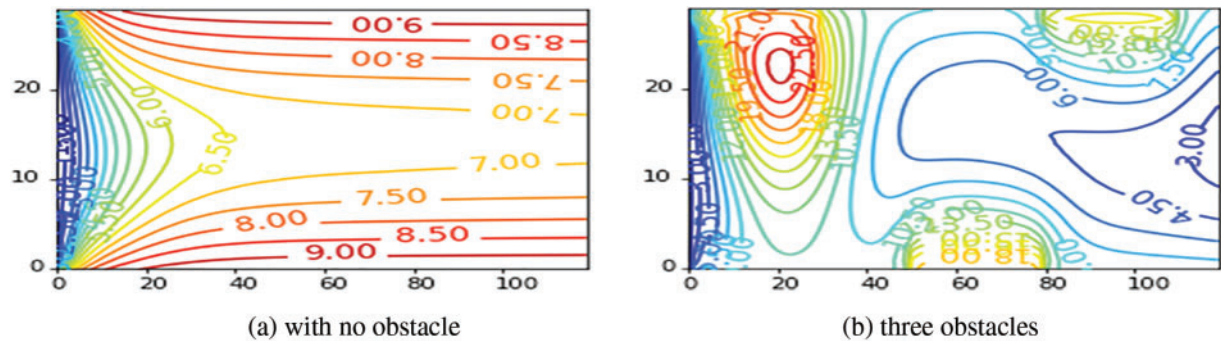
**Figure 7:** Velocity with nine obstacles for different  $Kn$  numbers

Fig. 9 illustrates the velocity contours for different cases with  $Kn = 0.05$  along the MC. In the absence of obstacles, in Fig. 9a, it can be seen that the velocity contours are parallel and increase symmetrically from the top and bottom walls of the MC to reach their maximum values at the MC center. In the other cases, Figs. 9b and 9c, the velocity contours are distorted around the obstacles, and they increase slowly from the developing region with higher values than in the previous case. It can be noticed that in the case with nine obstacles, Fig. 9c shows that the fluid flows slowly through the MC but accelerates as the exits. Analyzing these findings is crucial in evaluating the effectiveness of the obstacles installed in the MC with velocity slip and temperature jump. Furthermore, the study of the alterations caused by the obstacles in the velocity contours of the microchannel aids in enhancing the flow acceleration.



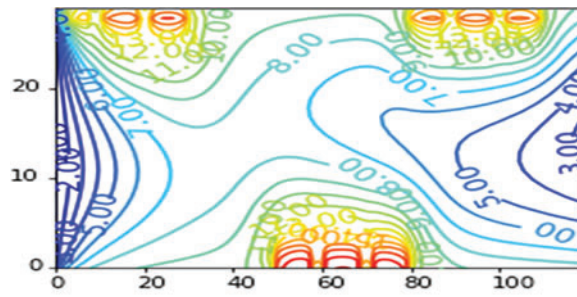
**Figure 8:** Velocity streamlines for  $Kn = 0.05$

Figs. 10–12 depict the distribution of temperature along MC for three scenarios with  $Kn$  values ranging from 0.012 to 0.05. The absence of obstacles in the first case exhibited a decrease in temperature with an increase in  $Kn$  number, as illustrated in Fig. 10. These outcomes indicate that the temperature of the fluid surges with the increase in dimensionless axial distance [28].



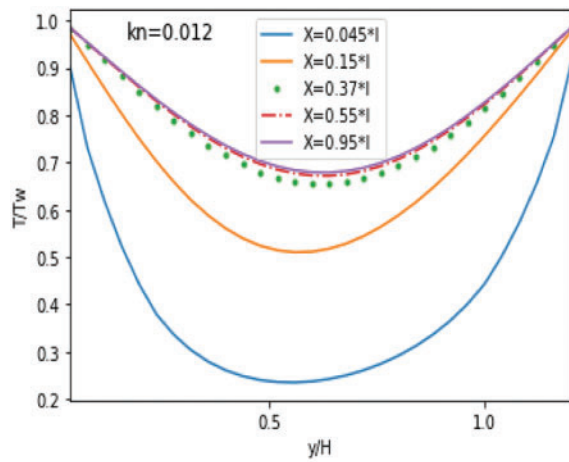
**Figure 9:** (Continued)



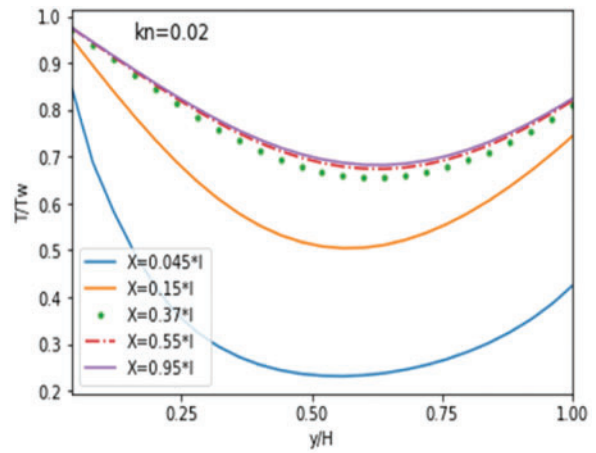


(c) with nine obstacles

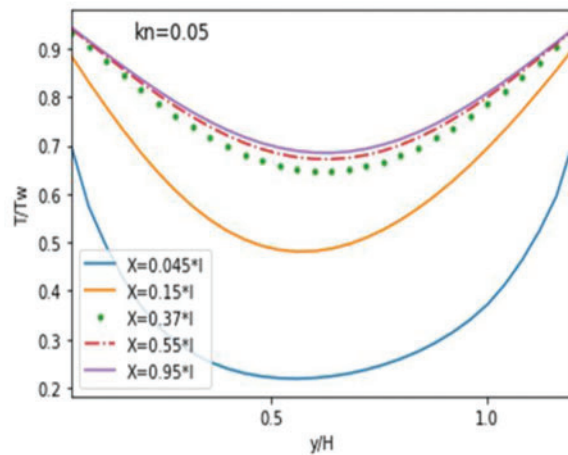
**Figure 9:** Velocity contours for  $Kn = 0.05$



(a)  $Kn = 0.012$



(b)  $Kn = 0.02$



(c)  $Kn = 0.05$

**Figure 10:** Evolution of the  $T$  according to different  $Kn$  numbers: Case with no obstacles



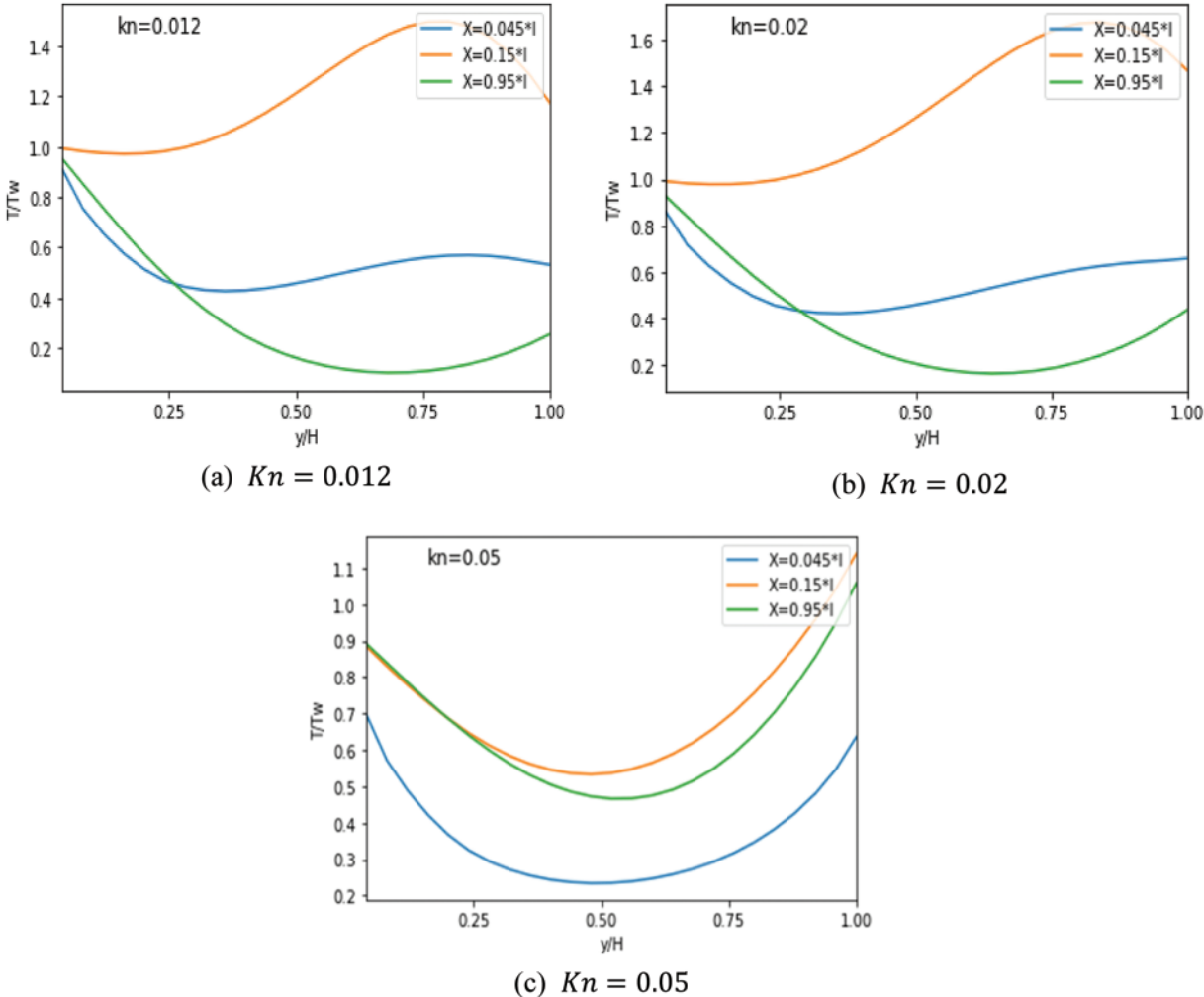


**Figure 11:** Evolution of the temperature according to different  $Kn$  numbers: Case with three obstacles

Even when adding obstacles, the temperature continues to drop. The temperature reduction is noticeable when nine obstacles are added, as seen in Figs. 12a and 12b, respectively. Moreover, the impact of rarefaction in the central area is more prominent compared to the region near the wall. This is attributed to the substantial temperature difference observed near the wall, which is caused by the rapid establishment of the hydrodynamic and thermal boundary layers in the entrance area, as depicted in Fig. 12. To sum it up, the MC with obstacles exhibits superior heat transfer enhancement in comparison to a smooth MC.

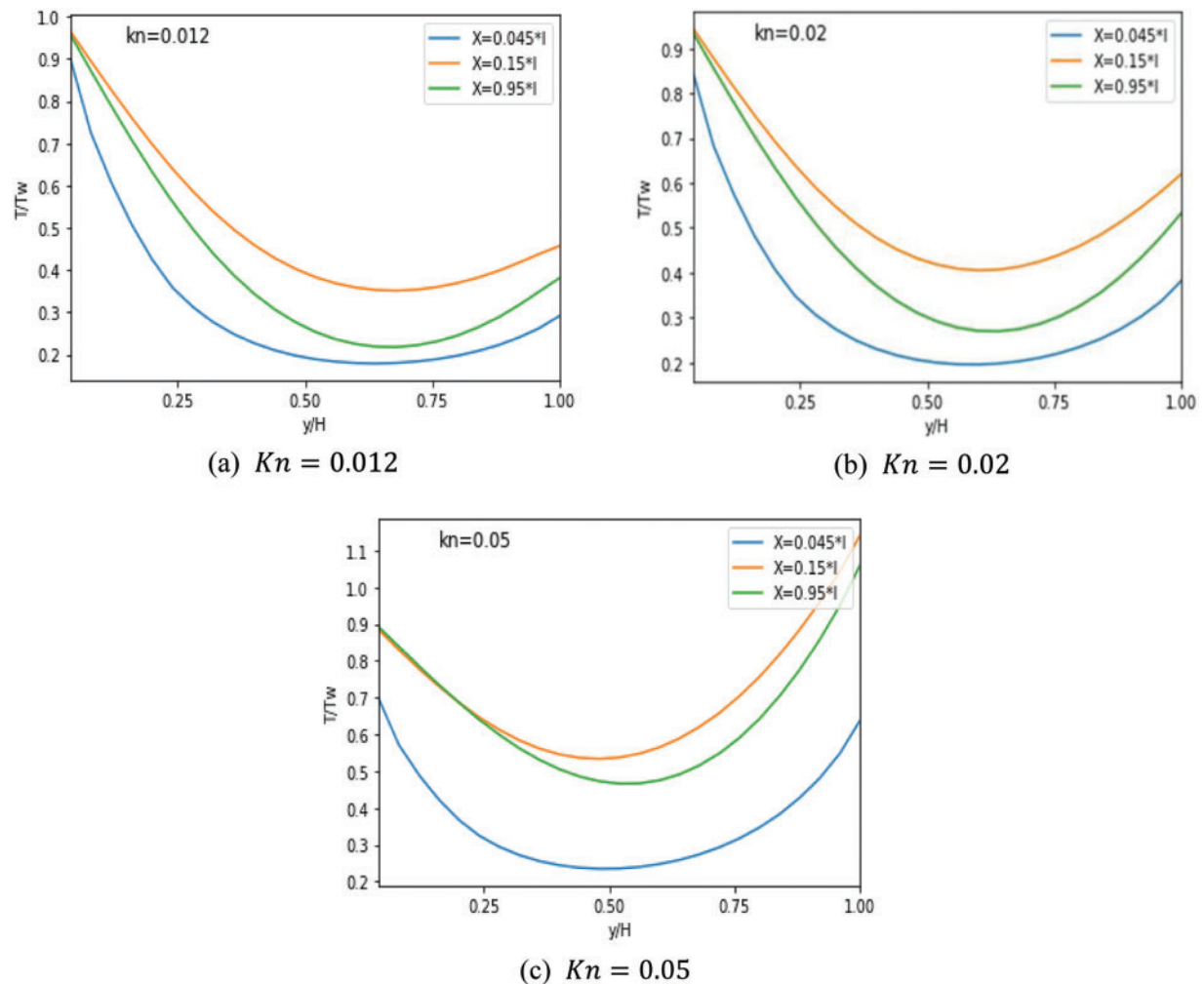


**Figure 12:** Evolution of the temperature according to different  $Kn$  numbers: Case with nine obstacles

From the streamlined Fig. 13, the temperature decreases rapidly from the wall to the neighboring layers, reaching a low value in the central region of the MC with no obstacles case, Fig. 13a. In the second case, Fig. 13b, the temperature near the first obstacle decreases slowly compared with other obstacles. But in the case with nine obstacles, the fluid flows quickly, as confirmed by the temperature profile, Fig. 13c. However, when compared to the scenario without obstacles, the inclusion of obstacles results in fluctuations in the temperature of the fluid at the wall and its adjacent layers. Furthermore, it leads to an increase in temperature in the central area of the MC.

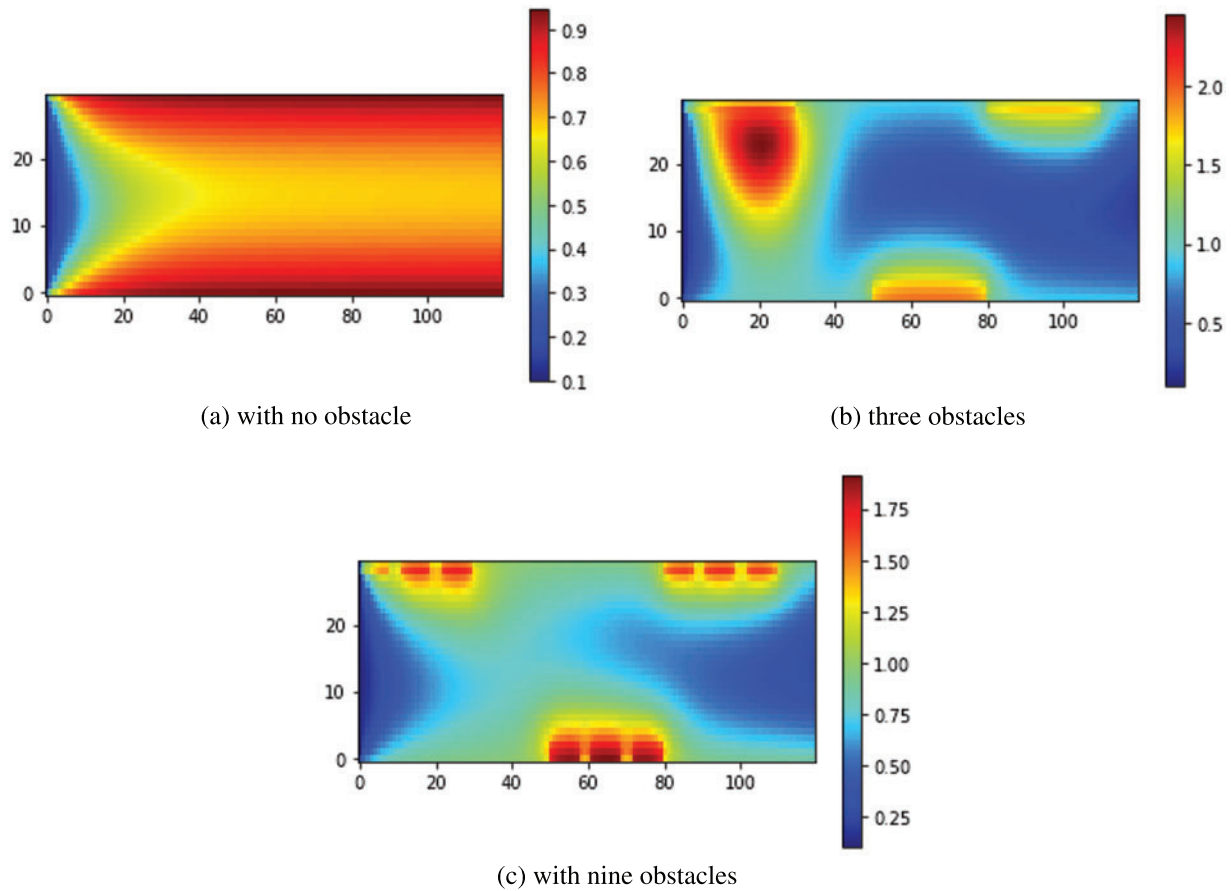


**Figure 13:** Functions of temperature streamlines for  $Kn = 0.05$

To illustrate the heat transfer improvement mechanism by obstacles, the temperature contour was added to the study. Fig. 14 depicts the temperature contours for  $Kn = 0.05$  along the MC. It can be seen that the temperature contours are parallel also. Their value increased in the central region with the absence of obstacles. The flow structure is noticeably different when obstacles are present. The figures show the heat transfer division between the obstacles in the other cases, Figs. 14b and 14c. In addition, the temperature contours are distorted, and a vortex is formed for the three obstacles case in the vicinity of the first obstacle. This vortex disappears for the nine obstacles case, Fig. 14c. However, low values are attained at the MC exit. And an increase in the temperature values along the MC is perceived with increasing the  $Kn$  number. These results are essential for assessing the overall efficacy of the obstacles installed in regulating the temperature of the MC. Moreover, the utilization of TLBM with a double distribution function enables the investigation of the thermal performance of rarefied flow in rectangular MCs with obstacles at varying  $Kn$  numbers while considering the slip velocity and temperature jump boundary conditions.

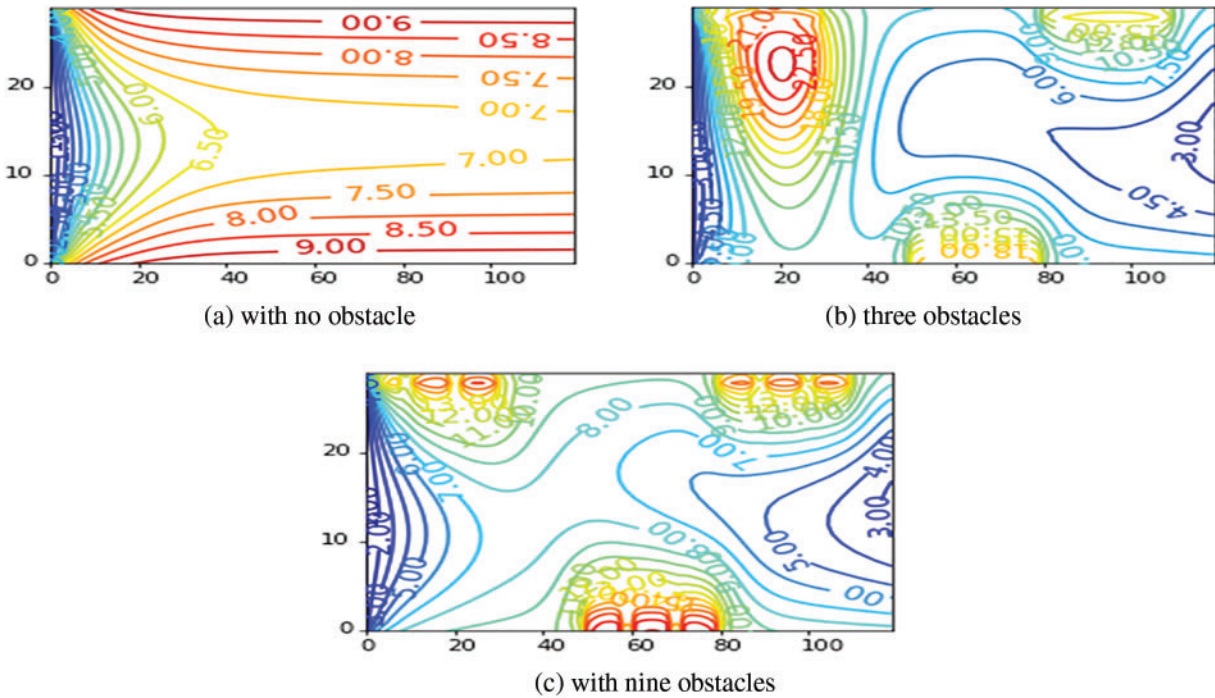


**Figure 14:** Temperature contours for  $Kn = 0.05$

The evolution of the  $Nu$  number according to various  $Kn$  numbers is shown in Fig. 15. The  $Nu$  number varies from 0.05 to 0.08 along the MC for the different studied cases. According to the obtained results, it is obvious that the  $Nu$  number reduces as the  $Kn$  number rises. The results show that even small  $Kn$  number values cause a great impact on the  $Nu$  number. The  $Nu$  number reached its maximum value at the MC's inlet.

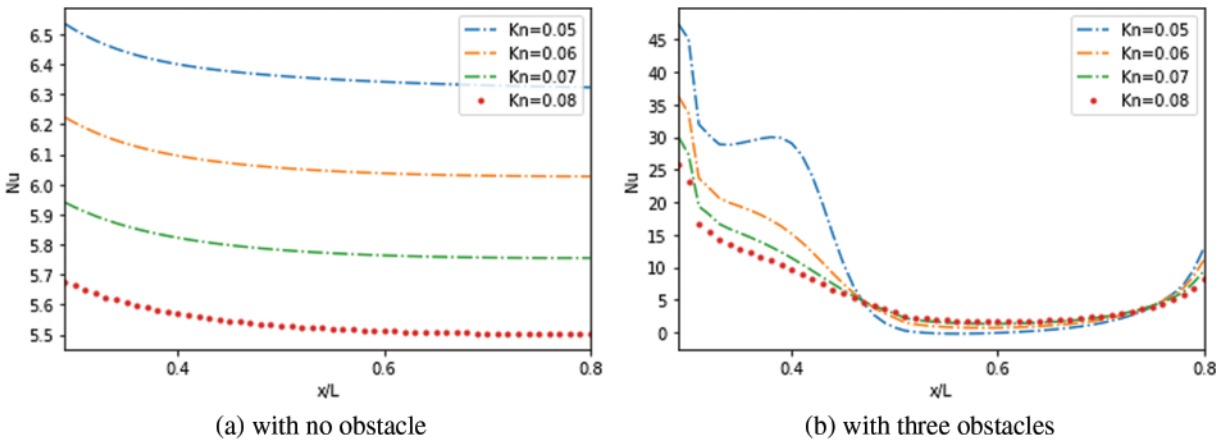
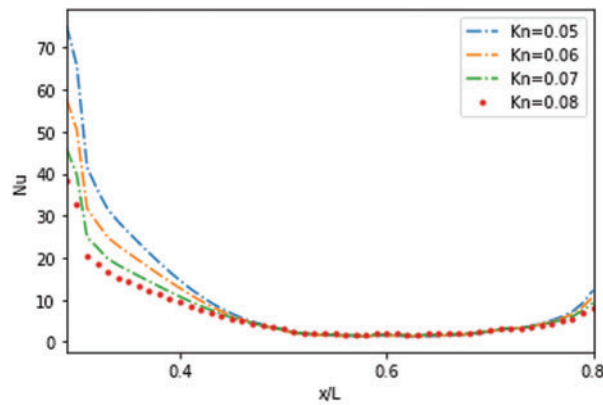


**Figure 15:** (Continued)

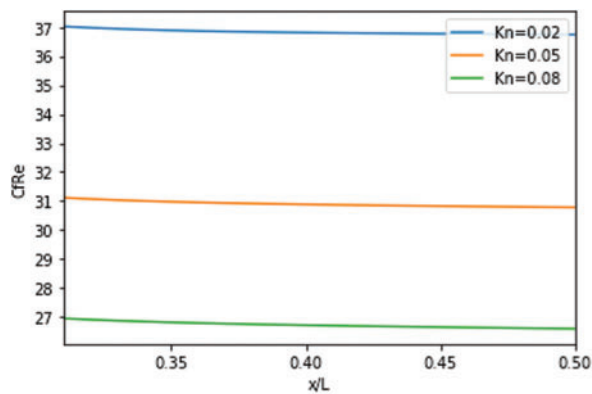


(c) with nine obstacles

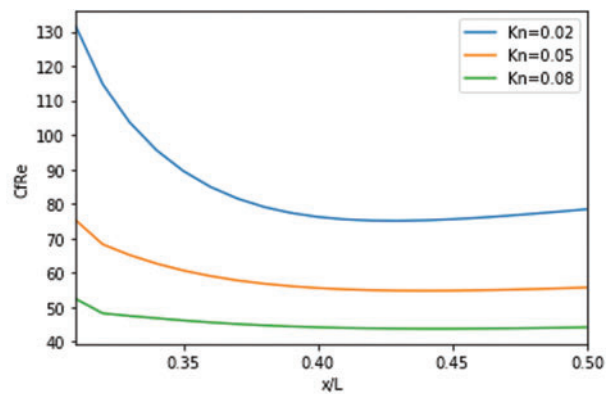
**Figure 15:** Effect of  $Kn$  number on  $Nu$  number

Furthermore, due to the temperature gradient at the entrance region, the highest values were reached in the second case compared to the third one. The  $Nu$  number's higher values denote that heat transfer is more efficient. Hence, rarefaction effects can substantially impact the  $Nu$  number in rarefied flows in the slip regime. From  $x = 0.6$ , the temperature gradient is almost constant for various  $Kn$  numbers in the second and third cases, so the rarefaction effect is no more predominant. In addition, the  $Nu$  number continues to reduce until the end of the MC [13]. Furthermore, from the results, conduction increases and convection decreases in the developing region.

Fig. 16 due to the rapid increase in velocity at the entrance zone and the reduction in the velocity gradient, the results showed a decreasing skin friction coefficient with a rise in  $Kn$  numbers according to the slip effect similar to [12]. Particularly, in case of no obstacles. However, the rarefaction effect was more significant in the second and third cases. The findings indicate that the third scenario, which incorporates nine obstacles in the microchannel, exhibits a superior reduction in the skin friction coefficient of the rarefied flow in the slip regime.

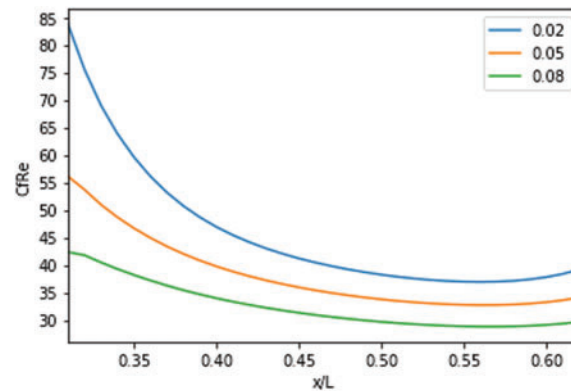


(a) with no obstacle



(b) with three obstacles

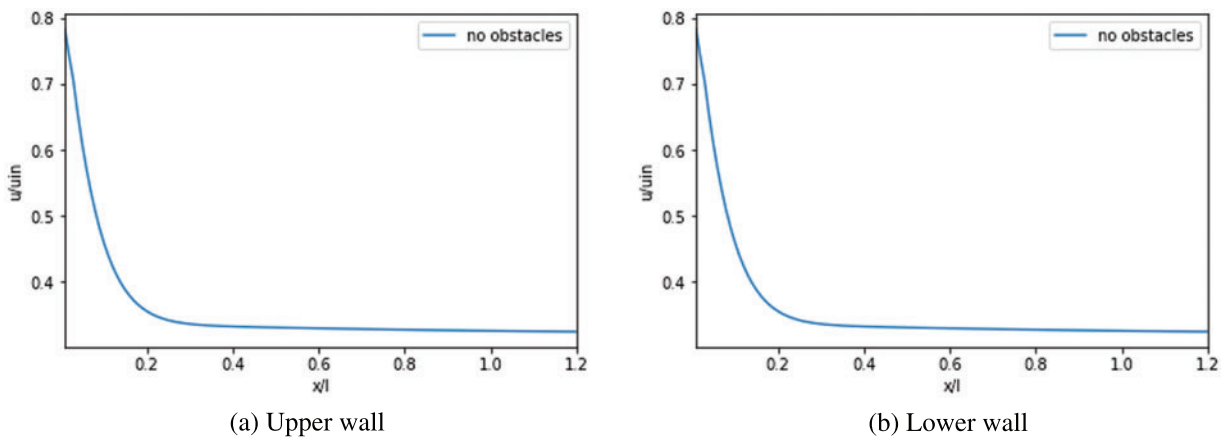
**Figure 16:** (Continued)



(c) with nine obstacles

**Figure 16:** Effect of  $Kn$  number on the friction coefficient

Figs. 17 to 19 illustrate the axial variation of velocity slip along the lower and upper wall for various  $Kn$  numbers. In the absence of obstacles, the velocity slip along the top and lower walls gradually decreases, Fig. 17. In the presence of obstacles, the velocity slip continues to decrease and is separated into zones based on the obstacle, the result of a dropping slip velocity related to velocity gradient reduction at the wall [12], Figs. 18 and 19. An increase in slip velocity occurs before the obstacle, followed by a decrease in slip velocity until it gets the minimal value at  $x = 0.6$  for the top wall and before  $x = 0.4$  for the bottom wall in the second and third cases, Figs. 18 and 19. The low value of velocity slip is related to the second case, Fig. 18.



(a) Upper wall

(b) Lower wall

**Figure 17:** Velocity slip: Case without obstacles

Figs. 20 to 22 depict the temperature jump along the upper and lower walls of the MC in the function of  $Kn$  number. In the developing region, the temperature jump keeps increasing rapidly in the absence of obstacles, Fig. 20. In the case of obstacles, the jumping temperature drops, and the low value of temperature jump occurs next to the obstacle. It increases when passing the obstacle. However, in both cases, with and without obstacles, the rarefaction effect does not influence the temperature jump on the top and bottom wall of MC for all  $Kn$  number values. Our study did not find any significant impact of rarefaction effect on temperature jump in slip regime of rarefied flow compared to other research such as [12].

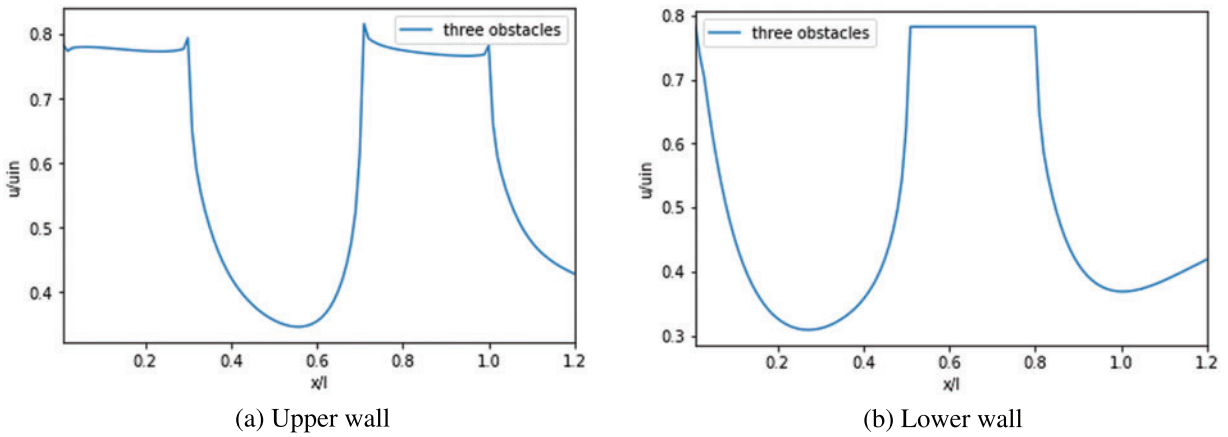


Figure 18: Velocity slip: Case with three obstacles

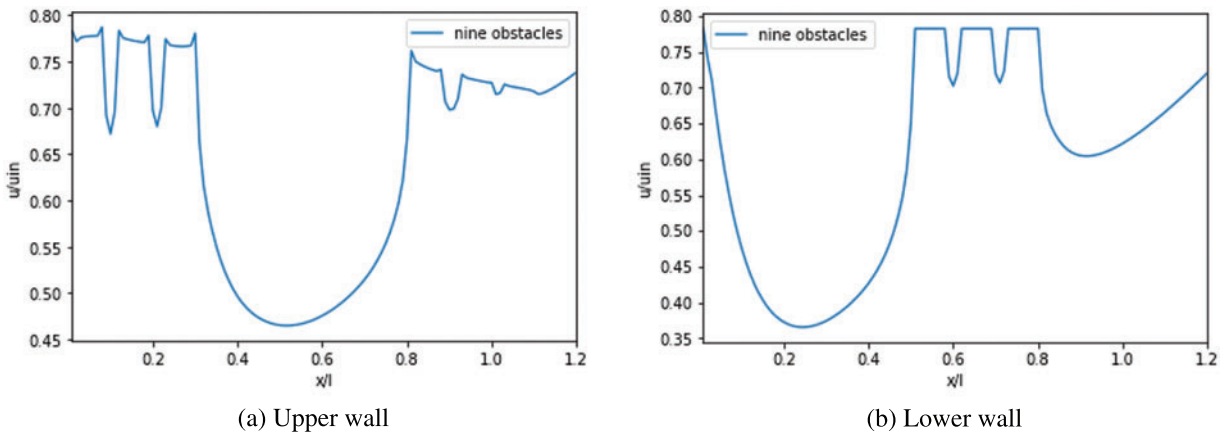


Figure 19: Velocity slip: Case with nine obstacles

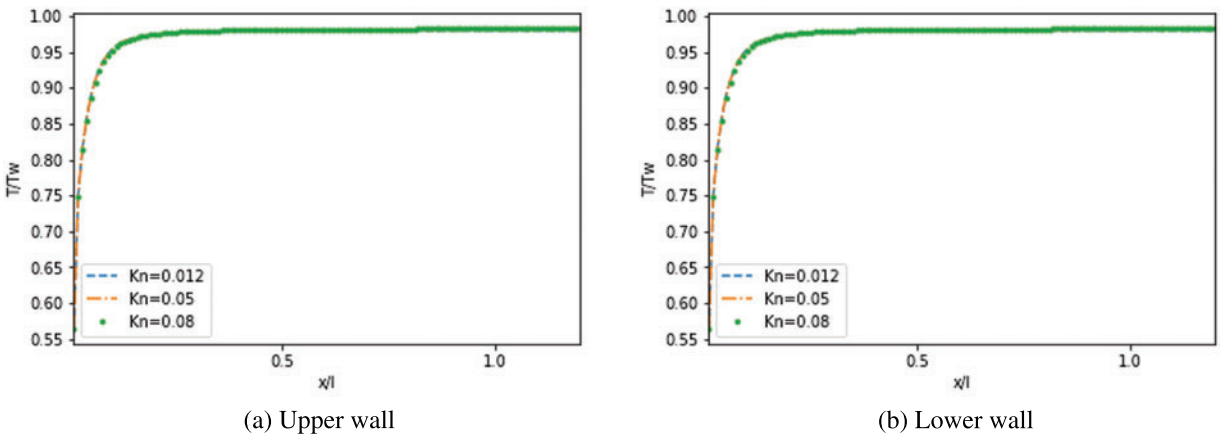
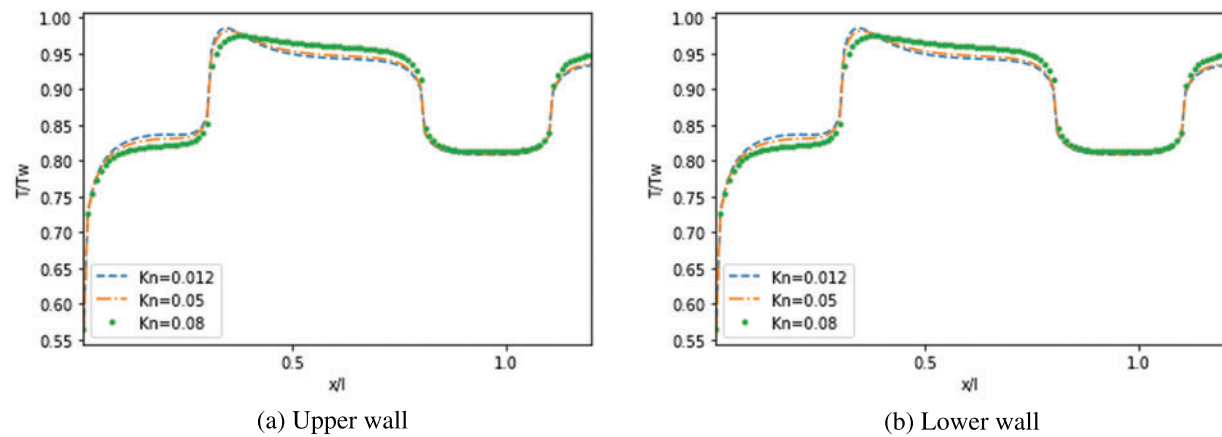
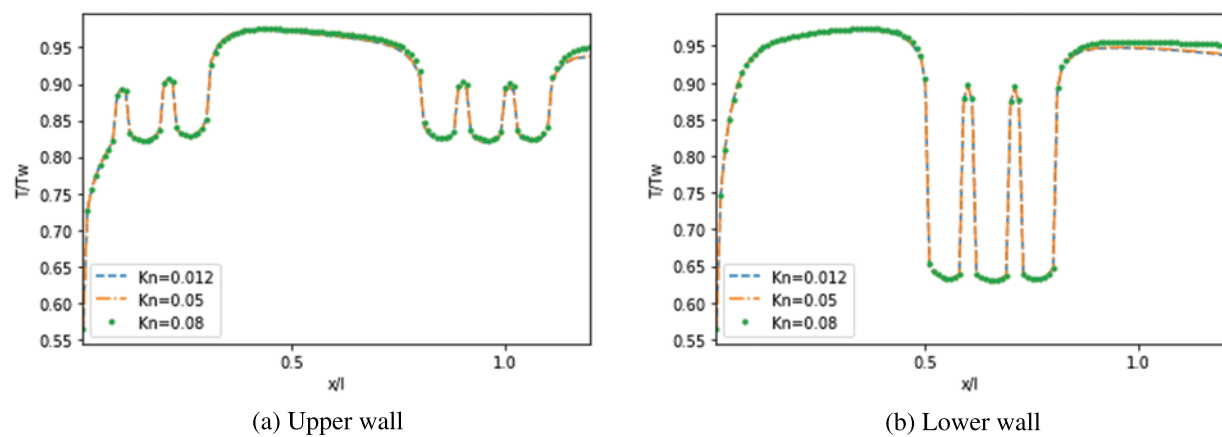


Figure 20: Effect of  $Kn$  number on the temperature jump: Case with no obstacles





**Figure 21:** Effect of  $Kn$  number on the temperature jump: Case with three obstacles



**Figure 22:** Effect of  $Kn$  number on the temperature jump: Case with nine obstacles

#### 4 Conclusions

The BGK model-based TLBM was employed using Python computing code to investigate forced convective heat and fluid flow in a unit length of a rectangular MC under three different configurations. The first configuration was without obstacles, while the second and third configurations featured three and nine obstacles, respectively. The temperature jump and slip velocity were considered at the boundary and extended to the obstacle level. This numerical investigation included an analysis of the impacts of temperature jump and velocity slip on heat transfer, temperature, and velocity profile, as well as the rarefaction effect's influence. The results showed the rarefaction effect's significance on velocity and temperature distribution. The current TLBM with a DDF allowed the modeling of MCs with and without obstacles with slip velocity and temperature jump. The study found that the fluid moved slowly through the third microchannel configuration (with nine obstacles) and accelerated at the MC outlet, as indicated by the lower temperature profile. No vortex was captured, but the results highlighted the critical role played by obstacles in MCs. Additionally, the rarefaction effect played a significant role in reducing the  $Nu$  number and skin friction coefficient in MCs containing obstacles.



Furthermore, the proposed configurations offer a solution for enhancing the microchannel geometry and utilizing microelectromechanical systems and microdevices as cooling techniques.

**Acknowledgement:** The authors express their appreciation to the General Directorate of Scientific Research and Technological Development (DGRSDT) of the Ministry of Higher Education and Scientific Research in Algeria.

**Funding Statement:** The authors received no specific funding for this study.

**Author Contributions:** The authors confirm contribution to the paper as follows: study conception: S. Hammid; study design: K. Naima; data collection: C. Kezrane; analysis and interpretation of results: K. Naima and A. Liazid; draft manuscript preparation: S. Hammid, K. Naima and Y. Menni; writing-review and editing: O.M. Ikumapayi, J. Asad, M.H. Rahman, F.L. Rashid, N.A. Hussien and Y. Menni. All authors reviewed the results and approved the final version of the manuscript.

**Availability of Data and Materials:** The data that support the findings of this study are available on request from the corresponding author.

**Conflicts of Interest:** The authors declare that they have no conflicts of interest to report regarding the present study.

## References

1. Mondal, B., Mehta, S. K., Pati, S., Patowari, P. K. (2021). Numerical analysis of electroosmotic mixing in a heterogeneous charged micromixer with obstacles. *Chemical Engineering and Processing-Process Intensification*, 168(432), 108585.
2. Rehman, K. U., Al-Mdallal, Q. M., Sherif, E. S. M., Junaedi, H., Lv, Y. P. (2021). Numerical study of low Reynolds hybrid discretized convergent-divergent (CD) channel rooted with obstructions in left/right vicinity of CD throat. *Results in Physics*, 24(2), 104141.
3. Ullah, Z., Ashraf, M., Sarris, I. E., Karakasidis, T. E. (2022). The impact of reduced gravity on oscillatory mixed convective heat transfer around a non-conducting heated circular cylinder. *Applied Sciences*, 12(10), 5081.
4. Lobasov, A. S., Minakov, A. V., Rudyak, V. Y. (2022). The investigation of the velocity slip and the temperature jump effect on the heat transfer characteristics in a microchannel. *Case Studies in Thermal Engineering*, 31(1), 101791.
5. Sun, L., Li, J., Xu, H., Ma, J., Peng, H. (2022). Numerical study on heat transfer and flow characteristics of novel microchannel heat sinks. *International Journal of Thermal Sciences*, 176(5), 107535.
6. Gao, J., Hu, Z., Yang, Q., Liang, X., Wu, H. (2022). Fluid flow and heat transfer in microchannel heat sinks: Modelling review and recent progress. *Thermal Science and Engineering Progress*, 29(2), 101203.
7. Xu, L., Yu, X., Regenauer-Lieb, K. (2020). An immersed boundary-lattice Boltzmann method for gaseous slip flow. *Physics of Fluids*, 32(1), 012002.
8. Yuan, Y., Rahman, S. (2016). Extended application of lattice Boltzmann method to rarefied gas flow in micro-channels. *Physica A: Statistical Mechanics and its Applications*, 463(4), 25–36.
9. Ahangar, E. K., Izanlu, M., Jabbari, M., Ahmadi, G., Karimipour, A. (2020). Thermal microscale gas flow simulation using wall function and bounce-back scheme: Modified lattice Boltzmann method. *International Communications in Heat and Mass Transfer*, 119(4), 104993.

10. Zhang, Y., Xie, G., Karimipour, A. (2020). Comprehensive analysis on the effect of asymmetric heat fluxes on microchannel slip flow and heat transfer via a lattice Boltzmann method. *International Communications in Heat and Mass Transfer*, 118, 104856.
11. D’Orazio, A., Karimipour, A. (2019). A useful case study to develop lattice Boltzmann method performance: Gravity effects on slip velocity and temperature profiles of an air flow inside a microchannel under a constant heat flux boundary condition. *International Journal of Heat and Mass Transfer*, 136(1), 1017–1029.
12. Zarita, R., Hachemi, M. (2018). Numerical investigation and analysis of heat transfer enhancement in a microchannel using nanofluids by the lattice Boltzmann method. *Frontiers in Heat and Mass Transfer*, 12(5), 1–12.
13. Javaherdeh, K., Karimi, H., Azarbarzin, T. (2021). Lattice Boltzmann simulation of fluid flow and heat transfer in a micro channel with heat sources located on the walls. *Superlattices and Microstructures*, 160(3), 107069.
14. Wang, K., Chai, Z., Hou, G., Chen, W., Xu, S. (2018). Slip boundary condition for lattice Boltzmann modeling of liquid flows. *Computers & Fluids*, 161(5), 60–73.
15. Li, L., Mei, R., Klausner, J. F. (2013). Boundary conditions for thermal lattice Boltzmann equation method. *Journal of Computational Physics*, 237, 366–395.
16. Yang, L., Yu, Y., Pei, H., Gao, Y., Hou, G. (2019). Lattice Boltzmann simulations of liquid flows in microchannel with an improved slip boundary condition. *Chemical Engineering Science*, 202(9), 105–117.
17. Sharma, K. V., Straka, R., Tavares, F. W. (2020). Current status of lattice Boltzmann methods applied to aerodynamic, aeroacoustic, and thermal flows. *Progress in Aerospace Sciences*, 115, 100616.
18. Niu, X. D., Shu, C., Chew, Y. T. (2007). A thermal lattice Boltzmann model with diffuse scattering boundary condition for micro thermal flows. *Computers & Fluids*, 36(2), 273–281.
19. Liu, X., Guo, Z. (2013). A lattice Boltzmann study of gas flows in a long micro-channel. *Computers & Mathematics with Applications*, 65(2), 186–193.
20. Hatami, M., Ganji, D. D. (2014). Thermal and flow analysis of microchannel heat sink (MCHS) cooled by Cu-water nanofluid using porous media approach and least square method. *Energy Conversion and Management*, 78(1), 347–358.
21. Ghadirzadeh, S., Kalteh, M. (2017). Lattice Boltzmann simulation of temperature jump effect on the nanofluid heat transfer in an annulus microchannel. *International Journal of Mechanical Sciences*, 133(1), 524–534.
22. Knupp, D. C., Mascouto, F. S., Abreu, L. A., Naveira-Cotta, C. P., Cotta, R. M. (2018). Conjugated heat transfer in circular microchannels with slip flow and axial diffusion effects. *International Communications in Heat and Mass Transfer*, 91(7), 225–233.
23. Ahangar, E. K., Ayani, M. B., Esfahani, J. A. (2019). Simulation of rarefied gas flow in a microchannel with backward facing step by two relaxation times using lattice Boltzmann method-slip and transient flow regimes. *International Journal of Mechanical Sciences*, 157, 802–815.
24. Alipour Lalami, A., Kalteh, M. (2019). Lattice Boltzmann simulation of nanofluid conjugate heat transfer in a wide microchannel: Effect of temperature jump, axial conduction and viscous dissipation. *Meccanica*, 54(1–2), 135–153.
25. Rehman, K. U., Al-Mdallal, Q. M. (2020). On partially heated circular obstacle in a channel having heated rectangular ribs: Finite element outcomes. *Case Studies in Thermal Engineering*, 18(10), 100597.
26. Ashraf, M., Ullah, Z. (2020). Effects of variable density on oscillatory flow around a non-conducting horizontal circular cylinder. *AIP Advances*, 10(1), 015020.
27. Qiu, T., Wen, D., Hong, W., Liu, Y. (2020). Heat transfer performance of a porous copper micro-channel heat sink. *Journal of Thermal Analysis and Calorimetry*, 139(2), 1453–1462.

28. Ma, H., Duan, Z., Ning, X., Su, L. (2021). Numerical investigation on heat transfer behavior of thermally developing flow inside rectangular microchannels. *Case Studies in Thermal Engineering*, 24(1), 100856.
29. Ashraf, M., Ilyas, A., Ullah, Z., Abbas, A. (2022). Periodic magnetohydrodynamic mixed convection flow along a cone embedded in a porous medium with variable surface temperature. *Annals of Nuclear Energy*, 175(1), 109218.
30. Lori, M. S., Vafai, K. (2022). Heat transfer and fluid flow analysis of microchannel heat sinks with periodic vertical porous ribs. *Applied Thermal Engineering*, 205(4), 118059.
31. Ganesh, N. V., Al-Mdallal, Q. M., Hirankumar, G., Kalaivanan, R. (2023). Effects of vertically embedded parallel hot elliptic obstacles inside a fully sinusoidal enclosure filled with SWCNT-water nanofluid. *International Journal of Thermofluids*, 17(19), 100276.
32. Yin, X., Zhang, J. (2012). An improved bounce-back scheme for complex boundary conditions in lattice Boltzmann method. *Journal of Computational Physics*, 231(11), 4295–4303.
33. Mohebbi, R., Delouei, A. A., Jamali, A., Izadi, M., Mohamad, A. A. (2019). Pore-scale simulation of non-Newtonian power-law fluid flow and forced convection in partially porous media: Thermal lattice Boltzmann method. *Physica A: Statistical Mechanics and its Applications*, 525(9), 642–656.
34. Samanta, R., Chattopadhyay, H., Guha, C. (2022). A review on the application of lattice Boltzmann method for melting and solidification problems. *Computational Materials Science*, 206(9–10), 111288.
35. Tian, Z. W., Zou, C., Liu, H. J., Guo, Z. L., Liu, Z. H. et al. (2007). Lattice Boltzmann scheme for simulating thermal micro-flow. *Physica A: Statistical Mechanics and its Applications*, 385(1), 59–68.
36. Zou, Q., He, X. (1997). On pressure and velocity boundary conditions for the lattice Boltzmann BGK model. *Physics of Fluids*, 9(6), 1591–1598.